

# Interpretable, similarity-driven multi-view embeddings from high-dimensional biomedical data

Brian B. Avants<sup>a</sup>, Nicholas J. Tustison<sup>a</sup>, James R. Stone<sup>b,b</sup>, and the Pediatric  
Imaging, Neurocognition and Genetics Study<sup>c</sup>

<sup>a</sup>*Department of Radiology and Medical Imaging, University of Virginia, Charlottesville, VA*

<sup>b</sup>*Department of Neurological Surgery, University of Virginia, Charlottesville, VA*

<sup>c</sup>*Data used in preparation of this article were obtained from the Pediatric Imaging, Neurocognition and Genetics Study (PING) database (<http://ping.chd.ucsd.edu>). As such, the investigators within PING contributed to the design and implementation of PING and/or provided data but did not participate in analysis or writing of this report. A complete listing of PING investigators can be found at <https://ping-dataportal.ucsd.edu/sharing/Authors10222012.pdf>*

---

## Abstract

---

Inter-modality covariation leveraged as a scientific principle can inform the development of novel hypotheses and increase statistical power in the analysis of diverse data. We present similarity-driven multi-view linear reconstruction (SiMLR), an algorithm that exploits inter-modality relationships to transform large scientific datasets into smaller, more well-powered and interpretable low-dimensional spaces. Novel aspects of this methodology include its objective function for identifying joint signal, an efficient approach based on sparse matrices for representing prior within-modality relationships and an efficient implementation that allows SiMLR to be applied to relatively large datasets with multiple modalities, each of which may have millions of entries. We first describe and contextualize SiMLR theory and implementation strategies. We then illustrate the method in simulated data to establish its expected performance. Subsequently, we demonstrate succinct SiMLR case studies, and compare with related methods, in publicly accessible example datasets. Lastly, we use SiMLR to derive a neurobiological embedding from three types of measurements - two measurements from structural neuroimaging complemented by single nucleotide polymorphisms (SNPs) from 44 depression and anxiety-related loci [1]. We find that, in a validation dataset, the low-dimensional space from the training set exhibits above-chance relationships with clinical measurements of anxiety and, to a lesser degree, depression. The results suggest that SiMLR is able to derive a low-dimensional representation space that, in suitable datasets, may be clinically relevant. Taken together, this collection of results shows that SiMLR

---

*Email addresses:* [stnava@gmail.com](mailto:stnava@gmail.com) (Brian B. Avants), [njt4n@virginia.edu](mailto:njt4n@virginia.edu) (Nicholas J. Tustison), [jrs7r@virginia.edu](mailto:jrs7r@virginia.edu) (James R. Stone<sup>b</sup>)

may be applied with default parameters to joint signal estimation from disparate modalities and may yield practically useful results.

*Keywords:* code:R, multi-modality embedding, brain, ANTs, ANTsR, genotype, depression, SiMLR, imaging genetics

## 1. Introduction

Healthcare – from both a prevention as well as treatment perspective – is increasingly turning to large, mixed datasets to gain a better understanding of the biological complexity that influences sensitivity or resistance to disease, injury, etc. In the case of rare diseases, multiview datasets are collected to build a more complete characterization of disease phenotype and potentially gain insights into etiology. In more common conditions, like Alzheimer’s disease, multiview datasets are motivated by the need to understand the diversity of the disease process, identify sub-groups and thereby advance personalized treatment approaches. Multiview data can also provide insight into the features that drive variability within the “normal” phenotype e.g. underlying factors that contribute to differences in neurobiological age [2].

Multi-view (or multiple modality) datasets are increasingly common in both preclinical and clinical neurosciences. In the idealized case, each view / modality will provide a completely unique measurement of the substrate biology. However, it is perhaps more common that each view provides a partial and not wholly independent perspective on a complex phenomenon. In this case, covariation can be exploited in order to sift through noisy measurements and better identify meaningful signal. Moreover, joint relationships across systems of the brain or across scale can form the foundation for integrative scientific hypotheses.

Pre-specified joint hypotheses allow the scientist to avoid a combinatorial explosion of tests for possible interactions. Although powerful in large enough, well-understood datasets, prior multivariate hypotheses can be difficult to enumerate with sufficient detail to support implementation and testing. Fully multivariate and data-driven dimensionality reduction models provide an alternative, including PCA: [3,4] and ICA: [5–7]. However, these popular models are not explicitly designed for interpretation across multiple modalities and do not provide an easy way for the scientist to regularize the solution with prior knowledge or to visualize the feature vectors which are both dense and signed (i.e. have both positive and negative weights).

Graph-regularized, imaging-focused dimensionality reduction methods emerged in recent years to address the desire for interpretable components [8–10]. **Graph-net** [10], similar to **SCCAN** [11,12], uses  $\ell_1$  regularization to constrain embedding vectors to be sparse and reduce over-fitting in high-dimensional problems. Non-negative factorization methods provide a second degree of interpretability by guaranteeing that factorizations are unsigned and, therefore, allow components to be interpreted in terms of their original units (e.g. millimeters) [13,14]. Other efforts [9,15] use prior constraints to guide solutions toward familiar sparsity patterns. More generally, regularization is also critical to well-posedness [16].

The need for joint, interpretable modeling of several ( $>2$ ) parallel but heterogeneous datatypes is rapidly increasing [17–21]. Multi-block data analysis methods such as Kettering’s five offerings [22] and more recent regularized generalized canonical correlation analysis (RGCCA) [23] and multiway generalized canonical correlation analysis [24] extend Hotelling’s classical CCA [25,26] to multi-view (viz. multi-block) data. Our contribution, similarity-driven multi-view linear reconstruction (SiMLR), is a joint embedding method – targeting scientific data – that links several of the ideas expressed in prior work. SiMLR builds on sparse canonical correlation analysis for neuroimaging (SCCAN) ([12,27,28]) and prior-based eigenanatomy [15,29]. SiMLR goes beyond SCCAN in that it takes two or more modalities as input, allows customized (graph) regularization models and uses a fast and memory efficient implementation appropriate for large datasets. SiMLR outputs locally optimal low-dimensional embeddings for each modality that best predict its partner modalities. SiMLR achieves this by reconstructing each modality matrix from a basis set derived from the partner modalities. One novel aspect of SiMLR is that the “linking” basis set can be computed with SVD, ICA or a simple sum while, simultaneously, the feature vectors may be constrained by both sparsity and non-negativity. Furthermore, the target energy (measuring the similarity between different modalities) is also flexible.<sup>1</sup>

The remainder of the text provides: (section 2) the theoretical and optimization framework for SiMLR within ANTsR; (section 3) a simulation study that clarifies both the assumptions behind SiMLR and its execution in software; (section 4) a brief review of publicly available examples; (section 5) an application to pediatric imaging genetics that identifies genotype-phenotype relationships with clinical depression and anxiety measurements.

## 2. Methodology: Similarity-driven multiview linear reconstruction

### 2.1 Software platform: ANTsR

The core platform, ANTsR, leverages the powerful R language to interface and help organize raw neuroimaging, genomics and other data. ANTsR uses Rcpp [30] to wrap Insight ToolKit (ITK, now in version 5 [31]) and ANTs (currently in version 2.3.3 [32]) C++ tools for the R environment. ANTsR is accessible via both github and neuroconductor [33] and is currently in version v0.5.6.2. Test data and readme files are available by typing `?simlr` from within ANTsR. The software used for this paper is available here <https://github.com/ANTsX/ANTsR/releases>.

### 2.2 Background methodology

We outline the terminology used in the technical discussion that follows.

- Multi-view: several modalities collected in one cohort; alternatively, the same measurements taken across different studies [34]. We focus on the first case here.

---

<sup>1</sup>SiMLR supports path modeling [Tenenhaus2010] but only the leave-one-modality-out approach is studied here.

- Covariation: we use the term in two contexts. As a general concept, we mean systematic changes in one modality are reflected in a predictable amount of change in other modalities. In the mathematical context, we use the definition of covariation for discrete random variables.
- Latent space/embeddings: both terms refer to an (often lower-dimensional) representation of high-dimensional data. These are also known as components in PCA. In the context of this paper, we are *approximating* the (hidden) latent space with the learned embeddings. Often, the true latent space cannot be known. We compute embeddings (or components), here, by multiplying feature vectors against input data matrices.
- Feature vectors: these are weights on the original features. In SiMLR, the feature vectors are the solutions that we are seeking. Projecting the feature vectors onto the original data will provide a low-dimensional representation.

We now discuss, briefly, the primary algorithms upon which SiMLR is based. We assume data matrices, below, are standardized (zero mean, unit variance) and  $\|\cdot\|$  denotes the Frobenius norm.

*Background: multiple regression*

Multiple regression solves a least squares problem that optimally fits several predictors (the  $n \times p$  matrix  $X$ ) to an outcome ( $y$ ). As a quadratic minimization problem, we have:

$$\arg \min_{\beta} \|y - X\beta\|^2,$$

with optimal least squares solution:

$$\hat{\beta} = (X^T X)^{-1} X^T y.$$

Above, we may also add a “ridge” penalty  $\lambda\|\beta\|^2$  on the  $\beta$ s which is useful if  $p \gg n$  i.e. in the case of complex, multi-view, multivariate datasets as we propose to model here.

*Background: Principal Component Analysis*

PCA, like multiple regression, may be formulated as the solution to an energy minimization problem. Select  $k < n$ , then find  $U$  ( $n \times k$ ),  $V$  ( $p \times k$ ) that minimize reconstruction error (where we add an  $\ell_1$  constraint as in [35–37] to illustrate *sparse* PCA):

$$\arg \min_{U,V} \|X - UV^T\|^2 + \sum_k \lambda_k \|V_k\|_1,$$

with additional constraints  $U = XV$  and  $V^T V = I$  where  $I$  is the identity matrix. The details of these constraints may vary in regularized variants of the method. Each of the columns of  $X$  is, here, expressed as a linear combination of the columns of  $U$ . For several modalities, we would compute:  $\{X_1 = U_1 V_1^T, \dots, X_n = U_n V_n^T\}$ . In this case, the “predictors” are the  $U_i$  and the  $V_i$  is analogous to the  $\beta$  in the multiple regression case. The  $V_i$  feature vectors will be sparse if the  $\ell_0$  or  $\ell_1$  penalty is used.

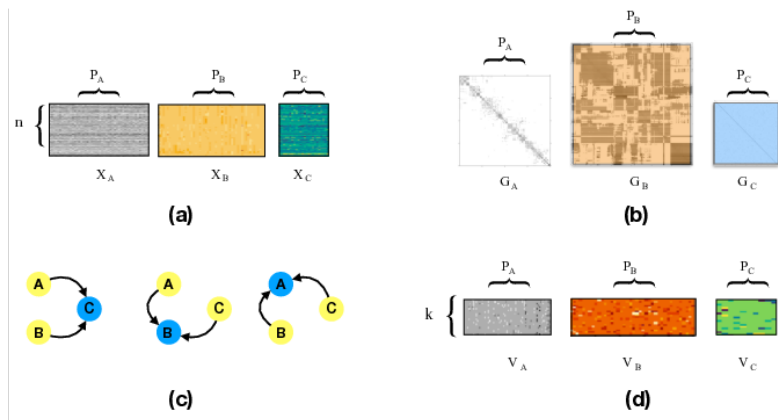


Figure 1: Overview of key components to SiMLR. Panel: (a) shows input data matrices for an example with 3 measurement types; (b) shows the associated graph-based regularization matrices where each is using a differing degree of regularization which is indicated by a greater or lesser degree of sparseness in the graph; (c) illustrates the optimization strategy where each basis set is used to estimate the left-out target matrix; (d) gives the  $k$  feature vectors, with sparse entries, that are output for each modality.

*Background: Canonical Correlation Analysis (CCA)*

CCA may be thought of as a generalization of multiple regression. Denote  $Y$  as a  $n \times q$  matrix. Then CCA seeks to find solution matrices  $U(k \times p), V(k \times q)$  that maximize correlation in a low-dimensional space:

$$\arg \max_{U,V} \text{tr}(\text{Corr}(XU^T, YV^T)),$$

where  $\text{Corr}$  is Pearson correlation and  $\text{tr}$  is the trace operator. In contrast to our previous formulation for PCA, CCA evaluates the objective function ( the “energy” ) in a reduced dimensionality space. Any of the methods above can be made sparse by enforcing the penalties on the feature weights as described for sparse PCA with the caveat that optimality constraints must be relaxed. Non-convex optimization methods such as alternating minimization and/or projected gradient descent must then be used [38–40].

### 2.3 Similarity-driven Multi-view Linear Reconstruction

SiMLR is a general framework that can be specified in forms that relate to either sparse PCA (a regression-like objective) or sparse CCA (a covariance-related objective). The primary concepts are illustrated in Figure 1. We make two assumptions about datasets to which we will apply SiMLR.

- **Assumption 1:** Real latent signal will manifest across the biological system on which we are collecting several measurements.

In such cases, methods that can link measurements across scales have a better chance of finding such signal; e.g. linking genetics, fluids, neuroimaging and cognition – in a statistically conservative model – is a primary motivation for using tools like those proposed here.

- **Assumption 2:** Multiview, regularized methods can reduce the impact of corrupted data.

It is likely that spurious signal will not be shared across all modalities – or all elements of the features within a modality – in a consistent manner. Natural filtering of noise occurs because (most forms of) noise does not covary across measurement instances. Adding regularization goes further in adding robustness: methods regularized with sparseness terms ( $\ell_0$  or  $\ell_1$ ) can down-weight (even to zero) features that do not improve the objective function. A caveat of these assumptions is that if no covariation across measurements exists – or if noise overwhelms all modalities/measurements – then these methods may not be relevant.

#### The SiMLR Objective Function

The core concepts in SiMLR include the fact that it incorporates flexible approaches to measuring differences between modalities (similarity-driven), can take as input several different matrices (multi-view) and that all operations are linear algebraic in nature (linear reconstruction). These properties are encapsulated in its objective function. SiMLR optimizes:

$$\arg \min_{V_i} \sum_i S(X_i, f(U_{\neq i}), V_i) + \text{Regularization}(V_i),$$

subject to:

$$\forall_i U_i = X_i V_i,$$

and for CCA-like  $S$ :

$$\|U_i\|_F = 1, \|V_i\|_F = 1,$$

where  $i$  ranges from 1 to the number of modalities (or views) and:

- $S$  - a function measuring the similarity of representations;
- $X_i$  - the  $n \times p_i$  matrix for a given measurement/view/modality;

- $U_{\neq i}$  - a  $n \times k$  low-dimensional representation of modalities other than  $X_i$ ;
- $V_i$  - a  $p_i \times k$  set of feature/solution vectors (analogous to  $\beta$ s) for the  $X_i$  modality;
- $f$  - a function estimating a low-rank basis set from its argument, described in more detail below.

The  $f(U_{\neq i}) = \tilde{U}_{\neq i}$  is a key novel component in the SiMLR framework and is derived by performing ICA, PCA, SVD or averaging over the set of  $j \neq i : \{X_j V_j\}$  embeddings. We now provide details for each term and other aspects of the implementation.

**Similarity Options.** The default similarity measurement is one of difference. This is akin to the reconstruction form for PCA, discussed above. In this case, we have:

$$S(X_i, \tilde{U}_{\neq i}, V_i) = \|X_i - \tilde{U}_{\neq i} V_i^T\|^2.$$

Here, SiMLR attempts to reconstruct each matrix  $X_i$  directly from the basis representation of the other  $n - 1$  modalities.

We also implement a similarity term inspired by CCA but modified for the SiMLR objective function. In prior work, we observed that the CCA criterion – in the under-constrained form here where we expect  $p \gg n$  – demonstrates some sensitivity to the sign of correlations [41]. As such, we implement an *absolute canonical covariance (ACC)* similarity measurement expressed as:

$$\frac{\text{tr}(|\tilde{U}_{\neq i}^T X_i V_i|)}{\|\tilde{U}_{\neq i}\| \|X_i V_i\|}.$$

The majority of our evaluation focuses on reconstruction error rather than ACC although we briefly touch on the covariance formulation in examples below. Both reconstruction and ACC have easily computable analytical derivatives that are amenable to projected gradient descent, as used in our prior work [11,12,15]. This similarity term is most closely related to SABSCOR and SABSCOV in multi-block data analysis [42,43].

The similarity also depends heavily on the selection for the basis representation. Any method for producing a basis set from the input matrices  $\{X_{j \neq i}\}$  would be valid. However, in practice, some methods will lead to more useful optimization landscapes than others. We provide four options in this initial work, at the implementation level.

- $f_{sum} = \sum_{j \neq i} U_j$
- $f_{svd} = \text{svd}_u([U_{j \neq i}])$
- $f_{ica} = \text{ica}_S([U_{j \neq i}])$ .
- $f_{alg-Orth} = \text{alg}([U_{j \neq i}])$  which combines *alg* with additional orthogonalization constraints.

$$\| \| X_C - f_{\text{alg}}( [ X_A \quad V_A^T ], X_B, V_B^T ) - V_C \|_F^2 + \ell_0( G_C V_C^T )$$

Figure 2: One term in SiMLR optimization. The modalities  $A$  and  $B$  are used to predict modality  $C$ . This example illustrates the reconstruction error / regression formulation and shows both the sparseness penalty and regularization applied to the solution feature vector for  $C$ .

The notation  $[U_{j \neq i}]$  indicates that we bind the columns together (cbind in R). The *alg* represents any of *svd*, *ica* or *sum*. The method *ica<sub>S</sub>* indicates that we take the  $S$  component of the ICA algorithm (where ICA produces  $X = AS$ ). The method *svd<sub>u</sub>* indicates that we take the  $U$  component of the SVD (where SVD produces  $X = UDV^T$ ). Figure 2 shows how these regularization terms interact with the reconstruction error in a visualization of one step of the optimization. Note: we focus on *ica<sub>S</sub>* as a mixing function for basis representations in this work as we have found that it produces useful outcomes in all of our example experiments.

**Regularization Options.** Regularization occurs on the  $V_i$  i.e. our feature vectors. Denote:

- $v_{ik}$  as the the  $k^{\text{th}}$  feature vector in  $V_i$ ;
- $G_i^\sigma$  as a sparse regularization matrix with rows that sum to one;
- $\gamma_i$  as a scalar weight.

Then the regularization terms take the form:

$$\text{Regularization}(V_i) = \sum_i \sum_k \gamma_i \|G_\sigma^i v_{ik}\|_{\ell_p}^+,$$

where  $\|\cdot\|_{\ell_p}^+$  is the positivity constrained  $\ell_p$  norm (usually,  $p = 0$  or  $p = 1$ ). This term both enforces sparseness via  $\ell_p$  while providing data-adaptive degrees of smoothing via the the graph regularization matrix  $G^i$ . For neuroimaging, this latter feature means that one does not need to pre-smooth images before running SiMLR. In practice,  $\|\cdot\|_{\ell_p}^+$  induces unsigned feature vectors. I.e. all non-zero entries will be either only positive or only negative.

**Regularization weights:** The parameterization of the sparseness for each modality is set by  $\gamma_i$  in the range of zero to one, where higher values are increasingly sparse (more values of the feature vector are zero). By default,  $\gamma_i$  is automatically set to accept the largest 50<sup>th</sup> percentile weights but the user may decide to increase or decrease this value depending on the needs of a specific study. Alternatively, one may use hyperparameter tuning methods to automatically determine  $\gamma_i$ . For most applications, we recommend default values.

**Regularization matrices:** optional  $G_\sigma^i$  are currently set by the user and must be determined in a data/application/hypothesis-specific manner. In implementation, we provide helper functions that allow the user to employ  $k$ -nearest neighbors (KNN) to set the (potentially large) regularization matrices. We use HNSW [44] to compute sparse KNN matrix representations for the  $G_\sigma^i$ . HNSW is among the most efficient methods currently available and, combined with sparse matrix representations, make graph regularization on large input matrices efficient. This aspect of regularization promotes smooth feature vectors where the nature of smoothness is typically determined by proximity either spatially or in terms of feature magnitude or feature correlation.

Although we provide default methods, choice of regularization should involve some consideration on the part of the user. Because there is no single theoretically justified answer to these questions, the best general approach would be to use hyper-parameter optimization. Alternatively, domain-specific knowledge may be used to guide parameter setting, in particular sparseness and regularization. Rules of thumb should be, for regularization, that the estimated  $V_i$  should appear to reflect biologically plausible feature sets. For sparseness, biological plausibility should also be considered although we believe our default parameters provide good general performance. As such, regularization (i.e. construction of the  $G_i$ ) should perhaps be given more domain-dependent attention by users. Examples below provide clarity on how we set these terms in practice. E.g. in neuroimaging, we may use  $k = 5^d$  mask-constrained neighbors for KNN where  $d$  is image dimensionality. For genomics or psychometrics data, we may set regularization simply by thresholding correlation (or [linkage disequilibrium](#) [45]) matrices.

*SiMLR: Optimization*

The overall approach to optimizing the SiMLR objective is that of projected gradient descent [46]. Here, one computes the optimization algorithm without regularization constraints and then, at each iteration, projects to the sub-space defined by the regularization terms. The SiMLR objective function for  $V_i$ , at a given iteration, depends only on the set values for  $X_i$  and  $\tilde{U}_{\neq i}$ . As such, we only need the gradient of the similarity term with respect to  $V_i$  which greatly simplifies implementation. We optimize total energy  $E$  via a projected gradient descent algorithm:

$$\begin{aligned} & \text{loop until convergence:} \\ \forall_i V_i^{\text{new}} & \leftarrow H( G_\sigma^i \star (V_i - \partial S / \partial V_i \epsilon_i) ) \\ \forall_i \tilde{U}_{j \neq i} & \leftarrow \text{falg}( [ X_j V_j^{\text{new}} ]_{j \neq i} ) \end{aligned}$$

where:

- $[ X_j V_j^{\text{new}} ]_{j \neq i}$  is the collection of low-dimensional projections resulting from multiplying the feature vectors onto the data matrices where  $j \neq i$  indicates that the  $i^{\text{th}}$  projection is held out;
- $H$  is the thresholding operation which here is applied separately to each column of  $V_i$  (see the *iterative hard/soft thresholding* literature [40] and [46] which suggests that  $\ell_0$  penalties provide greater robustness to noise);
- $\epsilon_i$  is a gradient step parameter determined automatically by line-search over the total energy  $E$ .

Recall that  $\text{falg}$  is a dimensionality reduction step that reduces  $U_{j \neq i}$  to a  $k$ -column matrix. Here, we provide an example gradient calculation for our default reconstruction error:

$$\begin{aligned} S &= \|X_i - \tilde{U}_{\neq i} V_i^T\|^2, \\ \partial S / \partial V_i &= -2(X_i^T - V_i \tilde{U}_{\neq i}^T) \tilde{U}_{\neq i}, \end{aligned}$$

which allows updating the full  $V_i$  at each gradient step. Only energy improving steps are allowed ( arrived at by line search ) which yields convergence to a local fixed point.

*SiMLR: Parameters and Initialization*

We summarize default (recommended) parameters and preprocessing steps for the methodology.

- Matrix pre-processing will be performed automatically. Unless the user overrides default behavior, we transform each matrix such that:  $\forall X_i : X_i \leftarrow \frac{sc(X_i)}{np_i}$  where  $sc$  denotes scaling and centering. Normalizing by  $np$  controls the relative scale of the eigenvalues of each matrix.

- Number of components ( $k$ ) – The practice for setting these values is very similar to practice in PCA or SVD; it may be determined via statistical power considerations, cross-validation or set to be  $k = n - 1$ , one less than the number of subjects. This is a problem that undergoes active research [47].
- Similarity measurement – *evaluation and comparison of similarity choices is ongoing*; Trade-offs are comparable to choosing correlation versus Euclidean distance for vectors and better performance may be gained in a data-dependent manner. ACC is faster to compute.

SiMLR may be initialized with several different approaches:

- random matrices for all or for each individual modality;
- a joint ICA across concatenated modalities (recommended and default behavior);
- Any other initial low-rank basis set e.g. derived from RGCCA, etc which may be passed to the algorithm by the user;

Due to the fact that SiMLR cannot guarantee convergence to a global optimum (sparse selection is a *np-hard* problem), several different starting points should be evaluated when using SiMLR in new problems. This is in concordance with the theory of `multi-start` global optimization which we can only approximate in practice [48,49].

### 3. Learning data-driven embeddings with SiMLR: Simulation study

#### 3.1 Data representation and ANTsR/SiMLR Code

SiMLR assumes “clean” data as input. This data has no missing values and is structured in matrix format with each modality matched along rows. SNP data is often formatted this way after imputing to a common reference dataset such as the HapMap. In neuroimaging, we employ region of interest measurements or spatial normalization in order to map a high-dimensional image into this common representation. For example, if a brain template has  $p$  voxels within the cortex and the population contains  $n$  subjects, then the matrix representation of the population level voxel-wise, normalized cortical thickness map will be  $X_{\text{thickness}}$  with dimensions  $n \times p$ . SiMLR accepts  $n > 1$  sets of data organized in this manner. A study of  $k$  distinct modalities would have input matrices with dimensions  $n \times p_i$ , noting that  $p_i$  need not equal  $p_j$  for any  $i, j \in 1, \dots, k$ .

#### 3.2 Simulated data

SiMLR assumes that common *latent signal* exists across modalities and may be found by linear projections into a low-dimensional space. We construct simulated data that matches this setting by drawing  $k$  matrices from a multivariate distribution generated from a common low-dimensional basis (the true latent

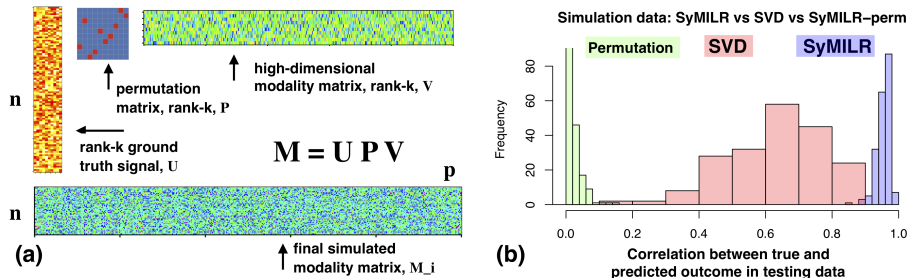


Figure 3: Simulation study. We simulate three high-dimensional modalities, each with a different number of columns, generated from a known ground truth low-dimensional signal. The ground truth matrix,  $U$ , is drawn from a multivariate gaussian distribution. SiMLR’s formulation suggests that the algorithm should be able to accurately recover the true signal from the three input high-dimensional data matrices. An example simulated matrix is shown in (a) where we detail the matrix construction process. The distribution of results, aggregated over 200 simulations, in (b) verifies that SiMLR exhibits reasonable recovery of the ground truth signal in testing data. As expected, singular value decomposition, performed independently on each of the three data matrices, does not perform as well. SVD performed jointly, i.e. run on the concatenated input matrices, recovers signal nearly as well as SiMLR. However, SVD run on corrupted concatenated matrices fails to recover the known signal while SiMLR maintains good performance.

signal), as illustrated in Figure 3. The evaluation criterion then compares the ability of SiMLR to recapture this known basis with respect to: (a) the singular value decomposition (SVD); (b) permutations of the original data. The former criterion will exhibit that SiMLR’s use of cross-modality information drives the solution closer to the ground truth basis in comparison to SVD. The second criterion contrasts the SiMLR solution to that which would be found when no covariation across modalities exists.

We run three experiments each of which is available in the script `simulationStudy.R` within [the github SiMLR examples repository](#). Experiment settings are determined by two parameters in the script: `compareToJointSVD` and `doCorruption`. The first parameter determines whether to run SVD independently on each of the three simulated input matrices or to use the concatenated matrices as in SUM-PCA [17]. The `doCorruption` parameter willfully corrupts half of the entries of the third simulated matrix input such that it has no relationship with the true simulated latent signal.

For each experiment, we run 20 simulations and evaluate the quality of the recovered signal by training a linear regression algorithm to relate the *learned* basis to the *true* basis. We then predict the latent signal in held-out test data (80 subjects are used for training and 20 for testing). In this scenario, better performing methods will lead to more accurate predictions of the latent signal in the testing subjects. We can evaluate, by paired *t*-test, whether SiMLR performs better than, equal to or worse than SVD.

- Experiment 1: independent SVD, no corruption. SiMLR outperforms

SVD producing a mean correlation with the true outcome of 0.929; SVD produces 0.637; The paired  $t$ -test yields  $t = 10.668, p = 1.839e - 09$ . SiMLR on permuted data yields a mean correlation with true outcome of -0.003689598. Output of this experiment is shown in the figure.

- Experiment 2: joint SVD, no corruption. SiMLR performs closely to joint SVD producing a mean correlation with the true outcome of 0.925; SVD produces 0.951; The paired  $t$ -test yields  $t = -1.6, p = 0.126$ . SiMLR on permuted data yields a mean correlation with true outcome of -0.013.
- Experiment 3: joint SVD, with corruption. SiMLR outperforms joint SVD producing a mean correlation with the true outcome of 0.888; SVD produces -0.01097541; The paired  $t$ -test yields  $t = 17.849, p = 2.493e - 13$ . SiMLR on permuted data yields a mean correlation with true outcome of 0.03590018. In this case, the mean variance explained by the SiMLR models (the  $U_{j \neq i}$ ) is reduced by roughly half for the corrupted matrix, as expected.

As expected, SiMLR is more robust to corrupted data and performs as well as the joint SVD does here in uncorrupted data. Joint SVD and SiMLR outperform the SVD run independently. Permuted results suggest no predictive signal can be learned. This latter result serves primarily as sanity check. Because this study is done in a training-testing format, these results are not due to over-fitting but due to the fact that SiMLR is able to uncover the ground truth result substantially more efficiently than the SVD in two of our experiments, as designed. We note that both the  $f_{\text{sum}}$  and  $f_{\text{ica}}$  choices for the mixing algorithm achieve overall similar results.

#### 4. SiMLR: Public data case studies

Case studies based on public data are available in [the github SiMLR examples repository](#). These reproducible studies demonstrate different practical uses for the tool as well as how one might setup data for and run an analysis based on SiMLR output. In addition to the simulation study described above, the repository hosts R markdown files that show how to apply SiMLR to neuroimaging, genetics (SNP, methylation and expression data) and phenotype/demographic variables. We encourage the interested reader to examine and run the studies but summarize two of the examples here providing a brief summary of the data, references and a qualitative review of the findings.

##### 4.1: SiMLR-regression in mouse genotype-phenotype data

Overview: This example is a two-view model that predicts mouse body mass index from SNPs using covariance-related dimensionality reduction criterion. It is based on pre-processed data provided in the BGLR R package [50]. We run both SiMLR and RGCCA on these data in order to compare these methods' ability to predict phenotype from genotype. We illustrate strategies that may be used in practice: (1) multiple starting points for SiMLR where we select the best one

based on explained variance; (2) regularization by linkage disequilibrium and  $\ell_1^+$ ; (3) adding optional orthogonality constraints [51]. Neither method is developed on or specialized for these data and, as such, this represents a relatively unbiased comparison. We did not seek to optimize either approach for this study but rather used defaults. We use the `SGCCA` function in `RGCCA` to compare with sparse generalized canonical correlation analysis as implemented in that package and with  $\ell_1$  sparseness settings that are a close match to `SiMLR` defaults, i.e. 0.5 for phenotype features and 0.1 (for `SGCCA`) and 0.9 (`SiMLR`) for the SNP feature vectors. These latter weights are roughly the same for each tool. We choose relatively high sparseness values in order to identify sparse “eigenSNPs”.

**Data:** The input data consists of 1,814 mice with 10,346 SNPs collected by the Wellcome Trust to support work on whole-genome regression and identifying quantitative trait loci related to diabetes. More details on these data and relevant references are provided in [50,52]. Of the available phenotype data, we select variables related to body mass index (BMI). The variable names are `Gender`, `Obesity.BMI`, `Obesity.BodyLength` and `EndNormalBW`. This leads to a 2-view problem such that  $X_{\text{phenotype}}$  (4 columns) is related to  $X_{\text{SNPs}}$  (10,346 columns) in the training data where  $n_{\text{training}} = 1,454$ . We define a training-testing split using our dimensionality reduction methods in supervised mode. As such, both tools produce a low-dimensional (3 components or embeddings total, one fewer than the number of phenotype predictors) representation of SNPs that can be plugged into a (here, random forest) regression model to predict the target outcome in the test data after training.

**Result:** Both `SiMLR` and `RGCCA` are effective in this “large-p-with-small-n” study. Prediction based on both gender and SNP predictors lead to correlations of  $\approx 0.5$  with the true BMI values. `SiMLR` achieves this while maintaining unsigned weights in the feature vectors. This 2-view genotype-phenotype example shows how a low-dimensional model may be learned from high-dimensional data to predict an outcome in a testing set. It also demonstrates how to select from multiple initializations based on examining the explained variance within the training data over a sequence of different initialization points. Figure~4 demonstrates the primary steps and results in this study. The top SNPs selected by `SiMLR` were rs3702854, rs13483748, rs13483759, rs13483766, rs13483927, gnfX.118.600.

#### 4.2: *SiMLR applied to PTBP neuroimaging data to investigate brain development*

**Overview:** This examples uses the *regression* similarity term and compares to the SVD. The pediatric template of brain perfusion (PTBP [53]) includes freely available multiple modality neuroimaging consistently collected in a cohort of subjects between ages 7 and 18 years of age. PTBP also includes a variety of demographic and cognitive measurements that can be compared to `SiMLR` embeddings. A relevant reference analysis of this data is available in [54].

**Data:** We provide pre-processed (machine learning ready) matrix format for three measurements taken in 97 subjects: voxelwise cortical thickness [55], fractional anisotropy (FA) derived from diffusion tensor imaging and cerebral blood

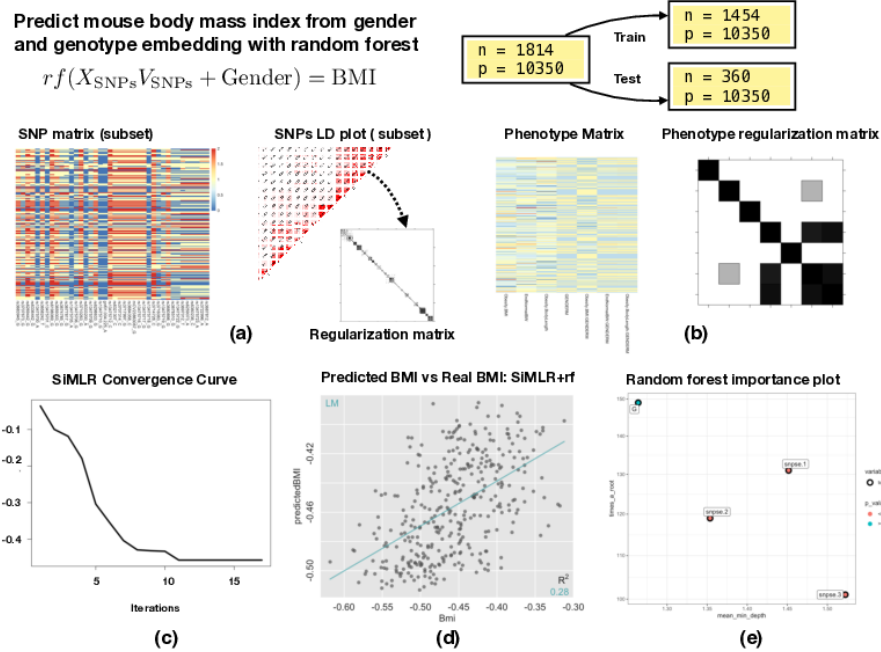


Figure 4: Predicting BMI from SNPs with random forest and SiMLR outputs. Panel (a) illustrates the SNP data input and regularization based on linkage disequilibrium. Panel (b) shows the phenotype input matrix and its regularization. Panel (c) provides a visual representation of the convergence of the total energy optimization. Panel (d) shows the multi-view prediction results for BMI based on SNP embedding vectors applied in testing data. Panel (e) is the multi-way importance plot from the `randomForestExplainer` package which demonstrates that each SNP embedding contributes significantly to the prediction.

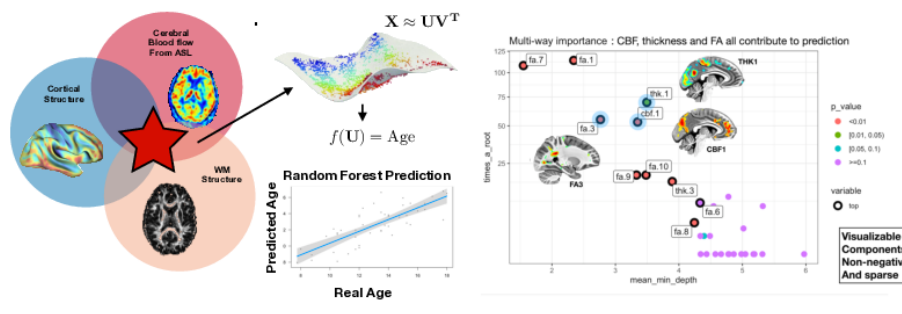


Figure 5: Predicting age from neuroimaging with random forest and SiMLR outputs. The left panel of the figure gives an overview of the study design. The right panel shows the multi-way importance plot from the `randomForestExplainer` package which demonstrates that each imaging embedding contributes significantly to the prediction.

flow (CBF) all at the voxel-wise level at 1mm resolution. The dimensionality of the matrices are  $97 \times 515,317$  for thickness and CBF and  $97 \times 438,394$  for FA.

Result: Both SiMLR and SVD component regression produce reasonable predictions of brain age [56] and related measurements in the PTBP. For comparison, in a given 50/50 train-test split of the data, the SiMLR age prediction error varies between 1.3 to 1.6 years as does SVD. These values are competitive with those reported in [54]. Furthermore, SiMLR embeddings relate more reliably with IQ measurements and SES scores, though with only marginal effect sizes. Relative to SVD, SiMLR feature vectors are more easily visualized and interpreted because (a) they are sparse and (b) they maintain their assignment to each input modality and the associated units of measurement. This example also illustrates an automated rank selection method based on permutation, as suggested in [57]. Figure~5 demonstrates the overall study design and the interpretability of the results.

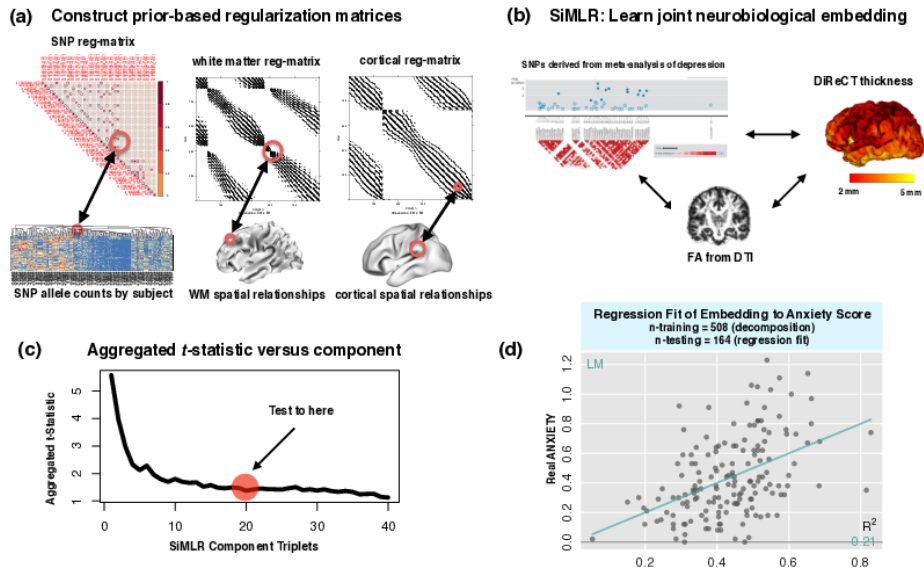


Figure 6: Depression and imaging genomics study overview. Panel (a) identifies the nature of the regularization used here, i.e. spatial regularization based on the cortical and white matter manifolds and regularization based on linkage disequilibrium for the SNP data. Panel (b) provides a visual representation of the learning process. Panel (c) demonstrates our selection process for the number of embeddings to test against anxiety and depression scores. Panel (d) shows the multi-view prediction results for anxiety based on thickness, FA and SNP embedding vectors applied in testing data. The thickness and SNP based embeddings contribute the most. The fit to depression scores is similar though less significant under permutation tests.

## 5. Learning data-driven embeddings with SiMLR: Imaging genomics

The key to this application demonstration is a recently reported analysis of genetic risk variants in depression [1]. Wray, et. al. provide chromosomal regions for 44 genetic loci associated with depression based on a large collection of data (135,458 subjects with major depression and 344,901 controls). This report allowed us to extract SNPs from these regions in an independent pediatric dataset (PING, described below) which also provides neuroimaging and, in a subset of subjects, clinical depression and anxiety scores. SiMLR will relate PING genotype to imaging phenotype and produce an embedding — from subjects without depression scores — that may be tested for predictive power in separate subjects that do have depression scores. The *testing* sample in no way overlaps with the training sample, although these subjects are selected from the same overall PING cohort.

### 5.1 PING Data

Data used in the preparation of this article were obtained from the Pediatric Imaging, Neurocognition and Genetics (PING) Study database (<http://ping.chd.ucsd.edu/>). PING was launched in 2009 by the National Institute on Drug Abuse (NIDA) and the Eunice Kennedy Shriver National Institute Of Child Health & Human Development (NICHD) as a 2-year project of the American Recovery and Reinvestment Act. The primary goal of PING has been to create a data resource of highly standardized and carefully curated magnetic resonance imaging (MRI) data, comprehensive genotyping data, and developmental and neuropsychological assessments for a large cohort of developing children aged 3 to 20 years. The scientific aim of the project is, by openly sharing these data, to amplify the power and productivity of investigations of healthy and disordered development in children, and to increase understanding of the origins of variation in neurobehavioral phenotypes. For up-to-date information, see <http://ping.chd.ucsd.edu/>. Data collection and sharing for this project was funded by the Pediatric Imaging, Neurocognition and Genetics Study (PING) (National Institutes of Health Grant RC2DA029475). PING is funded by the National Institute on Drug Abuse and the Eunice Kennedy Shriver National Institute of Child Health & Human Development. PING data are disseminated by the PING Coordinating Center at the Center for Human Development, University of California, San Diego.

For this example analysis, we divided the  $n = 670$  PING subjects with the required measurements into age-matched training ( $n = 508$ ) and testing ( $n = 162$ ) cohorts based on a simple criterion: the presence of both a summary clinical measurement of anxiety (Screen for Child Anxiety Related Emotional Disorders – Revised (AED)) and a second measurement of depression (Center for Epidemiological Studies Depression Scale for Children (CES-DC)). Table 1 shows relevant demographic variables for this split cohort. All subjects in both training and testing had three additional measurements: dense voxel-wise measurements of cortical thickness (derived from ANTs tools, v2.2.0 and following [58,59]), dense voxel-wise measurements of fractional anisotropy in white matter as well as a set of SNPs associated with depression via prior genome-wide meta analysis [1]. The normalized cortical thickness and FA images contain 66,565 and 68,966 voxels, respectively. We extracted 4,309 candidate SNPs from imputed PING data using default settings of the open-source software Plink [60]. Many of these SNPs exhibit known associations with neural processes and/or brain development, as described in annotations provided by [1].

Table 1: Demographics Table: The table details group characteristics for primary covariates in the training and testing groups. No significant differences exist. Note that depression and anxiety measures are only available within the testing group.

Predictor	trainGroup	testGroup	pValue
Age	14.6 ± 3.9	14.2 ± 3.8	0.338
Gender=F/M	240 (47.2%)/268	82 (50.0%)/82	0.6
parental education	5.7 ± 1.2	5.9 ± 1.1	0.06
parental income	6.8 ± 2.5	7.1 ± 2.3	0.11

Predictor	trainGroup	testGroup	pValue
CES-DC	NA	$0.7 \pm 0.5$	NA
AED	NA	$0.44 \pm 0.27$	NA

*Regularization matrices:* For the cortical and FA data, we employ a sparse gaussian regularization matrix, shown in Figure 6, that is based on spatial proximity along the cortical and white matter manifolds, respectively, as in previous studies [8]. This matrix is constructed automatically, given the sigma of the desired gaussian. For the SNP regularization matrix, we employ a similar approach but, instead of spatial proximity, use the linkage disequilibrium between SNPs. We normalize each row of the regularization matrices such that they sum to one.

*Regularization and initialization parameter setting:* Because we have a clear train-test split — and our ultimate goal is to relate brain structure and SNPs to clinical scores of anxiety and depression — we are able to select parameters based on (1) data-driven measurements, (2) prior knowledge and (3) the minimum total SiMLR energy over several different initializations. First, data-driven analysis from a helper function given in the examples above (and as described in [57]) suggests we choose a rank of 99 bases. This is likely to be overparameterized (given the regularization and the noise associated with SNPs) and, as such, we only perform inferential testing in a subset of these bases (strategy described below). Second, prior knowledge informs the selection of regularization matrix parameters, as described in previous sections. We tune the regularization matrices such that the solution,  $V_{ij}$ , represent plausibly smooth neuroanatomical networks when represented in the image/brain space. Using (3) is akin to a multi-start optimization method which reduces sensitivity to local minima. We search over 20 initial starting solutions and select the one with the best variance explained as the source of basis functions for application to the test data. After selecting the best model from the multi-start, we select the number of components to test. To assist this, we use ANTsR function `predictSiMLR` which summarizes the predictive capacity of each component for each modality. Several summary measures are included, in particular overall variance explained (averaged over all entries in each matrix) and the mean  $t$ -statistic for each component. As shown in Figure 6, we then plot the mean  $t$ -statistic over each component set i.e. the mean of ( thickness component- $k$ - $t$ -statistic + FA component- $k$ - $t$ -statistic + SNP component- $k$ - $t$ -statistic ). Inspecting this curve shows relatively little improved descriptive capability beyond 20 components/embeddings. We therefore test for associations between embeddings and anxiety/depression outcomes in the first 20 components.

## 5.2 Results

### 5.2.1 Relevance of low-dimensional embeddings to depression and anxiety

SiMLR is applied, above, as an unsupervised dimensionality reduction method operating on thickness, FA and SNPs. The resulting components can then

be tested for associations with other measurements which we do, here, in an independent sub-cohort of PING. The key to such an approach is that none of the target outcome data is visible to the dimensionality reduction algorithm. An analogous traditional method is [principal component regression](#).

We adopt a step-wise procedure to determine whether the SiMLR component regression demonstrates association with anxiety or depression scores. We assess the following candidate models in testing data:

- m-b: the base model is CES-DC or AED  $\approx age + gender + pedu + inc + gaf + scanner$  where *pedu* indicates parental educational level (in years) and *inc* denotes parental income. Four scanner types are included as factors to mitigate the effect of scanner variability. Six genetic ancestry factors are also included via the *gaf* variables. These control for potential ethnic or racial differences in the population sampling.
- m-f: adds  $X_{\text{thickness}}V_{\text{thickness}}^k$ ,  $X_{\text{FA}}V_{\text{FA}}^k$  and  $X_{\text{SNPs}}V_{\text{SNPs}}^k$  as predictors to m-b.

We assess such models for each  $k$  (i.e. over the 20 sets of triplet components) and compute empirical  $p$ -values by permutation. I.e. we test the ANOVA(m-b,m-f)  $F$ -score in the original data and compare the result to ANOVA(m-b,m-f) $_p$   $F$ -score in permuted data. This gives insight as to whether the additional set of basis vectors augments prediction while accounting for loss of degrees of freedom. Figure 6 panel (d) shows a scatter-plot of the prediction and the variance explained for the m-f model of AED. We perform 5,000 permutations for each  $k$ . The table of permutation-based  $p$ -values for each score and each component is in Table~2. For the best component (11), permutation-based assessment leads to a  $p$ -value of 0.0 (effectively  $< 2e-4$ ) for anxiety and 0.001 for the depression scores. The empirical  $p$ -values derive from the frequency at which the permuted embedding model performance exceeds the omnibus model from original data. No instance of the permuted embeddings exceeded the original data for anxiety scores.

Results are shown in Table 2 and indicate that a subset of embeddings contributes predictive value for both AED and CES-DC, in particular for components 1, 6, 11 with the latter representing the strongest effects. Investigating the raw regression models suggests that FA does not add substantial value to the score prediction. SNPs and thickness are consistently useful in both cases. Note that this is a post-hoc observation in that we have not explicitly tested for the significance of thickness versus SNPs or FA. We only test the triplets as a group. Two nuisance predictors reach marginal significance with age and GAF3 at  $p$ -value 0.014.

Table 2: Three components survive correction for multiple comparisons out of 20 (components columns). p-Val-Dep indicates raw permutation-based  $p$ -values for the depression score. q-Val-Dep indicates Bonferroni corrected  $p$ -values. p-Val-Anx indicates raw permutation-based  $p$ -values for the anxiety score with  $q$  indicating Bonferroni correction.

component	p.Val.Dep	q.Val.Dep	p.Val.Anx	q.Val.Anx
6	0.003801	0.07602	2e-04	0.004
11	0.002601	0.05201	2e-04	0.004
14	0.006401	0.128	0.0018	0.03601

### 5.2.2 Visualization/Interpretation

Sparse methods have the value of balancing the exploratory spirit of traditional machine learning tools (e.g. SVD) while retaining some of the interpretability and localization of hypothesis-driven (or univariate) designs. In the current example, we gain interpretability by being able to visualize the embedding vectors in the brain and SNP spaces, respectively, as in Figure 7. In the case of the brain, as in SNPs, identifying the anatomical location of the weights of the embedding vectors can yield further insight. Table 3 shows a breakdown of the relative anatomical contributions and locations of the weighted anatomy in the most predictive thickness embeddings. Insula emerges as the most highly weighted region and has been implicated in several prior studies of depression and cortical anatomy [61]. While it is tempting to focus on this individual region, it only contributes 30% of the total weight whereas the remainder of the signal is distributed across other medial, frontal and temporal areas. Furthermore, note that regularization matrices guarantee that signal is distributed across each of the domains of interest. This process gives a smoothly varying embedding vector (as can be seen in the brain spaces in Figure 7) and prevents over-fitting and isolated non-plausible high-weight entries.

Table 3: The anatomical coordinates of the primary cortical embedding vector. Over half of the signal is attributable to the left and right insula, the rolandic operculum, the right middle and superior temporal gyrus and the anterior cingulate. MNI coordinates and volume, weighted by the embedding vector weights, are also reported. Anatomical labels are derived from the AAL label set in ANTsR (see `data(aal)`) [62]. `cwts` refers to the cumulative contribution of the regions including and preceding the given row. `weightedVolume` is in  $\text{mm}^3$ . A similar table could be constructed for embedding vectors related to the SNP data.

anat	weightedVolume	cwts	coord.1	coord.2	coord.3
Frontal_Inf_Orb_R	2514	0.07205	-33.68	-29.41	-15.55
Calcarine_L	2405	0.141	5.915	75.57	5.01
Fusiform_L	2294	0.2067	32.64	25.55	-30.72
Temporal_Inf_L	2114	0.2673	50.47	40.78	-24.52
Fusiform_R	1854	0.3205	-30.95	7.645	-37
Frontal_Mid_R	1679	0.3686	-37.38	-52.28	23.87
Lingual_L	1616	0.4149	10.15	71.83	-7.783
Frontal_Inf_Orb_L	1586	0.4604	27.17	-21.58	-20.23
Temporal_Pole_Mid_L	1535	0.5044	26.91	-12.65	-39.85

anat	weightedVolume	cwts	coord.1	coord.2	coord.3
Rectus_R	1452	0.546	-5.77	-32.24	-21.81
Rectus_L	1445	0.5874	6.416	-27.29	-21.78
Temporal_Inf_R	1442	0.6288	-43.08	3.556	-39.46
Temporal_Pole_Mid_R	1188	0.6628	-32.56	-12.55	-36
Temporal_Pole_Sup_R	1123	0.695	-40.51	-15.32	-21.98
Frontal_Sup_Orb_R	1107	0.7267	-13.85	-43.57	-19.44
ParaHippocampal_L	1096	0.7581	22.37	9.386	-30.62
Temporal_Mid_R	1012	0.7872	-57.68	16.66	-10.47
Temporal_Pole_Sup_L	994.9	0.8157	30.05	-13.82	-30.55
Frontal_Sup_Orb_L	969.4	0.8435	12.3	-27.82	-23.42
Lingual_R	718.5	0.864	-6.843	71.17	-4.975
Precuneus_L	521.6	0.879	5.843	57.45	11.45
ParaHippocampal_R	427.8	0.8913	-25.17	8.606	-31.29
Frontal_Sup_R	328	0.9007	-25.27	-66.62	12.51
Calcarine_R	318	0.9098	-4.607	69.17	9.664
Frontal_Inf_Tri_R	304.8	0.9185	-45.89	-34.07	2.348
Cerebellum_Crus1_L	293.4	0.9269	45.61	54	-26.93
Temporal_Mid_L	236.2	0.9337	60.64	37.07	-2.092
Insula_R	216.6	0.9399	-31.08	-19.89	-13.55
Frontal_Med_Orb_R	211.5	0.946	-3.544	-33.22	-14.19

## 6. Discussion

This paper details SiMLR, an algorithm for computing sparse and regularized neurobiological embeddings from high-dimensional, multiple modality datasets. We demonstrate its performance in simulated data that clearly matches its assumptions, how to run the algorithm from within ANTsR. We also share an application to an imaging genetics study of depression as well as two case studies that are covered more briefly. SiMLR embodies a class of methods to provide interpretable, graph-regularized, sparse and unsigned components from multi-view data. The methods that we develop are generalizations of classical methods like PCA and CCA, are efficient in high-dimensional data, build in network-based regularization, extend to an arbitrary number of modalities and can be used for hypothesis testing, clustering or inference. SiMLR was demonstrated and evaluated in studies relating imaging, genomics, cognition, demographics and other phenotypic datasets. We provide strategies for parameter setting, training and testing study design and the visualization and interpretation of results. The framework is open source and relevant to understanding complex, potentially subtle patterns in healthcare data.

Two case studies demonstrate – with both code and datasets – how one may use SiMLR with either covariance related or regression related similarity measurements. These examples are designed to show how scientists may adapt this tool for their own needs. The BGLR/BMI prediction study uses SiMLR as a tool for

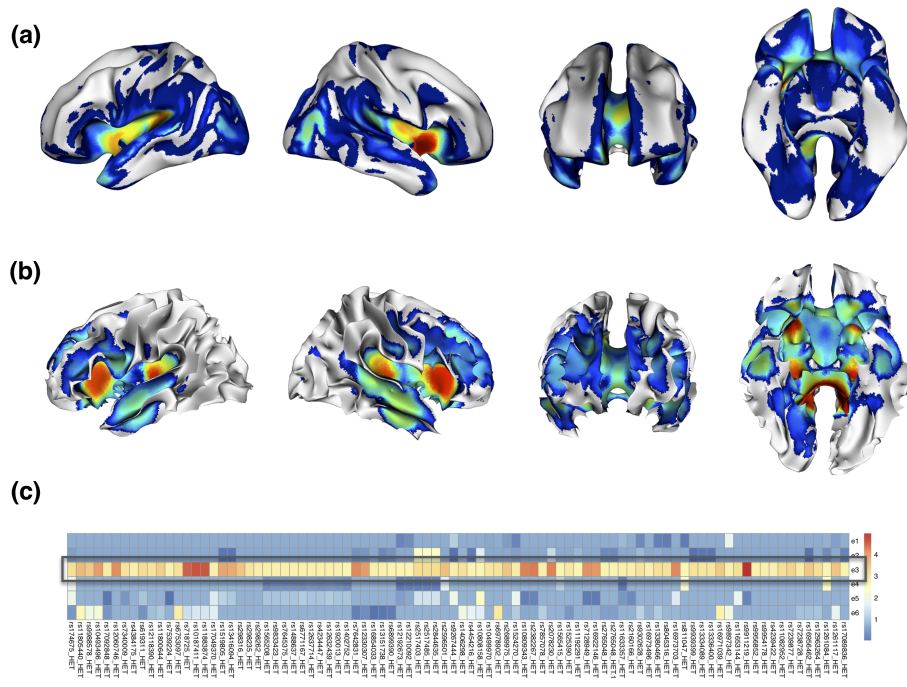


Figure 7: Visualization of high-dimensional embedding vectors. Panel (a) shows the most predictive thickness high-dimensional embedding vector. Panel (b) shows the same for the FA. Panel (c) illustrates the most highly-weighted SNPs. High weights should not be over-interpreted as they may represent algorithmic constraints as well as relevance to the representation.

supervised feature learning for a regression study. The learned embeddings are linked with a random forest to predict BMI in test data. Performance in this data is comparable to RGCCA although SiMLR provides additional regularization to the solution.

The PTBP study uses SiMLR purely as a dimensionality reduction tool in a manner identical to what one would do with PCA or SVD. The feature vectors are learned and then applied to inference or prediction problems. Relative to SVD, the SiMLR feature vectors lead to a stronger relationship with cognitive scores and comparable predictive value for the well-studied brainAge problem. We attribute the advantage to the locality of sparse feature vectors in comparison to the global features produced by SVD.

Interestingly, in both simulation and real clinical data, SiMLR appears to identify shared but not wholly redundant signal from high-dimensional multi-view data. In the PING study, cortical thickness and SNPs *jointly improve the prediction of CES-DC and AED*. This joint predictive power suggests that the neurobiological basis of depression may be distributed across several systems (cortex, connectivity and genotype) and scales (molecular to anatomical). This feature may also relate to the method’s core mathematics: high-dimensional embedding vectors are constructed purely from within modality data but the low-dimensional bases are derived from cross-modality representations. An advantage of this design is that SiMLR is easily applied to transfer learning, i.e. reusing knowledge from one domain in another. We note, though, that this will only be effective in datasets that exhibit some degree of cross-modality covariation. If not, then SiMLR may obscure rather than extract hidden signal and traditional or sparse SVD may be a better choice. However, our results show that SiMLR’s sparse feature vectors produce relationships with other metadata that are (at minimum) competitive with SVD. This may suggest that sparse methods that provide “increased locality” can be of value for identifying neurobiological patterns that may relate to clinical differences.

Given the abundance of research demonstrating substantial genetic risk in depression, it may be unsurprising that this work recapitulates these findings, albeit in a novel study design. The *joint structure* uncovered by SiMLR is perhaps unique to this study and may deserve further inquiry by scientists interested in detailing relationships between genotype, brain structure and clinical phenotype. It would be interesting, for instance, to examine how/if the polygenic relationship between genetics and depression/anxiety may be mediated by multivariate brain structure. However, these results should be approached with caution in that the datasets are relatively small and idiosyncratic. We believe this approach and the current findings will be strengthened by application in related datasets such as those provided by ABCD, the UK Biobank and Human Connectome Project. Furthermore, SiMLR is a recent method that will undergo refinement, validation and interpretation efforts in the near future.

This work provides several automated or semi-automated strategies for selecting regularization parameters and the rank ( $k$ ) for the feature vectors. However, we note that none of these strategies are “perfect” and that discussion continues about parameter setting even in more classical methodology (PCA,

CCA). While cross-validation approaches may also be used, the computational and data expense for these is relatively high and they also suffer theoretical as well as practical limitations in terms of effectiveness [47]. Despite these issues that are rather general, we believe the current implementation and interface to `SiMLR`, combined with guidance provided here, may yield a practically useful tool for multiple modality analysis of biomedical imaging and related data.

A second caveat to this study is that the design is explicitly multivariate and, as such, we do not interrogate the predictive value of individual embeddings. Our statistical focus is on the omnibus models. Other researchers may prefer to study individual embeddings independently. This is one known limitation within the current application of `SiMLR`.

Beyond the formulation and implementation of the method, accessibility of the algorithm is a key contribution. `ANTsR` is available in `github` and via the `neuroconductor` software distribution platform. Thus, `SiMLR` is available for near immediate access to users who are familiar with the `R` computing environment and who wish to test its applicability in their own data. As always, we recommend interested users contact developers/authors for guidance or with issues arising in the use of this software.

## Support

This work is supported by the Office of Naval Research N00014-18-1-2440.

## REFERENCES

1. Wray NR, Ripke S, Mattheisen M, Trzaskowski M, Byrne EM, Abdellaoui A, et al. Genome-wide association analyses identify 44 risk variants and refine the genetic architecture of major depression. *Nature Genetics*. 2018. doi:[10.1038/s41588-018-0090-3](https://doi.org/10.1038/s41588-018-0090-3)
2. Cole JH, Marioni RE, Harris SE, Deary IJ. Brain age and other bodily ‘ages’: implications for neuropsychiatry. 2019. doi:[10.1038/s41380-018-0098-1](https://doi.org/10.1038/s41380-018-0098-1)
3. Habeck C, Stern Y, Alzheimer’s Disease Neuroimaging Initiative. Multivariate data analysis for neuroimaging data: overview and application to Alzheimer’s disease. *Cell Biochem Biophys*. 2010;58: 53–67. doi:[10.1007/s12013-010-9093-0](https://doi.org/10.1007/s12013-010-9093-0)
4. Shamy JL, Habeck C, Hof PR, Amaral DG, Fong SG, Buonocore MH, et al. Volumetric correlates of spatiotemporal working and recognition memory impairment in aged rhesus monkeys. *Cereb Cortex*. 2011;21: 1559–1573. doi:[10.1093/cercor/bhq210](https://doi.org/10.1093/cercor/bhq210)
5. McKeown MJ, Makeig S, Brown GG, Jung TP, Kindermann SS, Bell AJ, et al. Analysis of fMRI data by blind separation into independent spatial components. *Hum Brain Mapp*. 1998;6: 160–188.
6. Calhoun VD, Adali T, Pearlson GD, Pekar JJ. A method for making group inferences from functional {MRI} data using independent component analysis. *Hum Brain Mapp*. 2001;14: 140–151.

7. Calhoun VD, Liu J, Adali T. A review of group {ICA} for f{MRI} data and {ICA} for joint inference of imaging, genetic, and {ERP} data. *Neuroimage*. 2009;45: S163—72. doi:[10.1016/j.neuroimage.2008.10.057](https://doi.org/10.1016/j.neuroimage.2008.10.057)
8. Avants BB. Relating high-dimensional structural networks to resting functional connectivity with sparse canonical correlation analysis for neuroimaging. 2018. doi:[10.1007/978-1-4939-7647-8\\_6](https://doi.org/10.1007/978-1-4939-7647-8_6)
9. Pierrefeu A de, Lofstedt T, Hadj-Selem F, Dubois M, Jardri R, Fovet T, et al. Structured Sparse Principal Components Analysis With the TV-Elastic Net Penalty. *IEEE transactions on medical imaging*. 2018;37: 396–407. doi:[10.1109/TMI.2017.2749140](https://doi.org/10.1109/TMI.2017.2749140)
10. Du L, Huang H, Yan J, Kim S, Risacher SL, Inlow M, et al. Structured sparse canonical correlation analysis for brain imaging genetics: an improved GraphNet method. *Bioinformatics (Oxford, England)*. 2016;32: 1544–1551. doi:[10.1093/bioinformatics/btw033](https://doi.org/10.1093/bioinformatics/btw033)
11. Avants B, Cook PA, McMillan C, Grossman M, Tustison NJ, Zheng Y, et al. Sparse unbiased analysis of anatomical variance in longitudinal imaging. *Med Image Comput Comput Assist Interv*. 2010;13: 324–331.
12. Avants BB, Libon DJ, Rascovsky K, Boller A, McMillan CT, Massimo L, et al. Sparse canonical correlation analysis relates network-level atrophy to multivariate cognitive measures in a neurodegenerative population. *Neuroimage*. 2014;84: 698–711. doi:[10.1016/j.neuroimage.2013.09.048](https://doi.org/10.1016/j.neuroimage.2013.09.048)
13. Lee DD, Seung HS. Learning the parts of objects by non-negative matrix factorization. *Nature*. 1999. doi:[10.1038/44565](https://doi.org/10.1038/44565)
14. Chalise P, Fridley BL. Integrative clustering of multi-level 'omic data based on non-negative matrix factorization algorithm. *PLoS ONE*. 2017. doi:[10.1371/journal.pone.0176278](https://doi.org/10.1371/journal.pone.0176278)
15. P.S. D, D.A. W, S.R. D, L.H. U, J.C. G, B.B. A, et al. Subject-specific functional parcellation via prior based eigenanatomy. *NeuroImage*. 2014.
16. Bell JB, Tikhonov AN, Arsenin VY. *Solutions of Ill-Posed Problems*. *Mathematics of Computation*. 1978. doi:[10.2307/2006360](https://doi.org/10.2307/2006360)
17. Smilde AK, Westerhuis JA, De Jong S. A framework for sequential multiblock component methods. *Journal of Chemometrics*. 2003. doi:[10.1002/cem.811](https://doi.org/10.1002/cem.811)
18. Tenenhaus A, Tenenhaus M. Regularized Generalized Canonical Correlation Analysis. *Psychometrika*. 2011. doi:[10.1007/s11336-011-9206-8](https://doi.org/10.1007/s11336-011-9206-8)
19. Tenenhaus M, Tenenhaus A, Groenen PJ. Regularized Generalized Canonical Correlation Analysis: A Framework for Sequential Multiblock Component Methods. *Psychometrika*. 2017. doi:[10.1007/s11336-017-9573-x](https://doi.org/10.1007/s11336-017-9573-x)
20. Zhan Z, Ma Z, Peng W. Biomedical Data Analysis Based on Multi-view Intact Space Learning with Geodesic Similarity Preserving. *Neural Processing Letters*. 2018; 1. doi:[10.1007/s11063-018-9874-9](https://doi.org/10.1007/s11063-018-9874-9)
21. Baltrusaitis T, Ahuja C, Morency LP. *Multimodal Machine Learning: A Survey and Taxonomy*. 2018. doi:[10.1109/TPAMI.2018.2798607](https://doi.org/10.1109/TPAMI.2018.2798607)
22. Kettenring JR. Canonical analysis of several sets of variables. *Biometrika*. 1971. doi:[10.1093/biomet/58.3.433](https://doi.org/10.1093/biomet/58.3.433)
23. Tenenhaus A, Philippe C, Guillemot V, Le Cao KA, Grill J, Frouin V. Variable selection for generalized canonical correlation analysis. *Biostatistics*. 2014. doi:[10.1093/biostatistics/kxu001](https://doi.org/10.1093/biostatistics/kxu001)

24. Arnaud Gloaguen , Cathy Philippe, Vincent Frouin, Giulia Gennari, Ghislaine Dehaene-Lambertz, Laurent Le Brusquet AT. Multiway Generalized Canonical Correlation Analysis. *Biostatistics*. 2020;In Press.
25. Hotelling H. Canonical Correlation Analysis (CCA). *J Educ Psychol*. 1935.
26. Hotelling H. Relations between two sets of variants. *Biometrika*. 1936; 321–377.
27. McMillan CT, Avants B, Irwin DJ, Toledo JB, Wolk DA, Van Deerlin VM, et al. Can MRI screen for CSF biomarkers in neurodegenerative disease? *Neurology*. 2013. doi:[10.1212/WNL.0b013e31827b9147](https://doi.org/10.1212/WNL.0b013e31827b9147)
28. McMillan CT, Toledo JB, Avants BB, Cook PA, Wood EM, Suh E, et al. Genetic and neuroanatomic associations in sporadic frontotemporal lobar degeneration. *Neurobiology of Aging*. 2014. doi:[10.1016/j.neurobiolaging.2013.11.029](https://doi.org/10.1016/j.neurobiolaging.2013.11.029)
29. Cook PA, McMillan CT, Avants BB, Peelle JE, Gee JC, Grossman M. Relating brain anatomy and cognitive ability using a multivariate multimodal framework. *NeuroImage*. 2014. doi:[10.1016/j.neuroimage.2014.05.008](https://doi.org/10.1016/j.neuroimage.2014.05.008)
30. Eddelbuettel D, Balamuta JJ. Extending R with C++: A Brief Introduction to Rcpp. *American Statistician*. 2018. doi:[10.1080/00031305.2017.1375990](https://doi.org/10.1080/00031305.2017.1375990)
31. Avants BB, Johnson HJ, Tustison NJ. Neuroinformatics and the the insight toolkit. 2015. doi:[10.3389/fninf.2015.00005](https://doi.org/10.3389/fninf.2015.00005)
32. Avants BB, Tustison NJ, Song G, Cook PA, Klein A, Gee JC. A reproducible evaluation of ANTs similarity metric performance in brain image registration. *NeuroImage*. 2011. doi:[10.1016/j.neuroimage.2010.09.025](https://doi.org/10.1016/j.neuroimage.2010.09.025)
33. Muschelli J, Gherman A, Fortin JP, Avants B, Whitcher B, Clayden JD, et al. Neuroconductor: An R platform for medical imaging analysis. *Biostatistics*. 2019. doi:[10.1093/biostatistics/kxx068](https://doi.org/10.1093/biostatistics/kxx068)
34. De Vito R, Bellio R, Trippa L, Parmigiani G. Multi-study factor analysis. *Biometrics*. 2019. doi:[10.1111/biom.12974](https://doi.org/10.1111/biom.12974)
35. Zou H, Hastie T, Tibshirani R. Sparse principal component analysis. *Journal of Computational and Graphical Statistics*. 2006. doi:[10.1198/106186006X113430](https://doi.org/10.1198/106186006X113430)
36. Shen H, Huang JZ. Sparse principal component analysis via regularized low rank matrix approximation. *Journal of Multivariate Analysis*. 2008. doi:[10.1016/j.jmva.2007.06.007](https://doi.org/10.1016/j.jmva.2007.06.007)
37. Jolliffe IT, Trendafilov NT, Uddin M. A Modified Principal Component Technique Based on the LASSO. *Journal of Computational and Graphical Statistics*. 2003. doi:[10.1198/1061860032148](https://doi.org/10.1198/1061860032148)
38. Lin CJ. Projected gradient methods for nonnegative matrix factorization. *Neural Computation*. 2007. doi:[10.1162/neco.2007.19.10.2756](https://doi.org/10.1162/neco.2007.19.10.2756)
39. Jain P, Netrapalli P, Sanghavi S. Low-rank matrix completion using alternating minimization. *Proceedings of the annual acm symposium on theory of computing*. 2013. doi:[10.1145/2488608.2488693](https://doi.org/10.1145/2488608.2488693)
40. Blumensath T, Davies ME. Iterative hard thresholding for compressed sensing. *Applied and Computational Harmonic Analysis*. 2009. doi:[10.1016/j.acha.2009.04.002](https://doi.org/10.1016/j.acha.2009.04.002)
41. Pustina D, Avants B, Faseyitan OK, Medaglia JD, Coslett HB. Improved accuracy of lesion to symptom mapping with multivariate sparse canonical correlations. *Neuropsychologia*. 2018;115: 154–166. doi:[10.1016/j.neuropsychologia.2017.08.027](https://doi.org/10.1016/j.neuropsychologia.2017.08.027)

42. Hanafi M. PLS Path modelling: Computation of latent variables with the estimation mode B. *Computational Statistics*. 2007. doi:[10.1007/s00180-007-0042-3](https://doi.org/10.1007/s00180-007-0042-3)
43. Tenenhaus A, Philippe C, Frouin V. *Computational Statistics and Data Analysis Kernel Generalized Canonical Correlation Analysis*. *Computational Statistics and Data Analysis*. 2015. doi:[10.1016/j.csda.2015.04.004](https://doi.org/10.1016/j.csda.2015.04.004)
44. Malkov YA, Yashunin DA. Efficient and Robust Approximate Nearest Neighbor Search Using Hierarchical Navigable Small World Graphs. *IEEE Transactions on Pattern Analysis and Machine Intelligence*. 2020. doi:[10.1109/TPAMI.2018.2889473](https://doi.org/10.1109/TPAMI.2018.2889473)
45. Hill WG, Robertson A. Linkage disequilibrium in finite populations. *Theoretical and Applied Genetics*. 1968. doi:[10.1007/BF01245622](https://doi.org/10.1007/BF01245622)
46. Bahmani S, Raj B. A unifying analysis of projected gradient descent for lp-constrained least squares. *Applied and Computational Harmonic Analysis*. 2013. doi:[10.1016/j.acha.2012.07.004](https://doi.org/10.1016/j.acha.2012.07.004)
47. Bro R, Kjeldahl K, Smilde AK, Kiers HA. Cross-validation of component models: A critical look at current methods. *Analytical and Bioanalytical Chemistry*. 2008. doi:[10.1007/s00216-007-1790-1](https://doi.org/10.1007/s00216-007-1790-1)
48. Martí R, Resende MG, Ribeiro CC. Multi-start methods for combinatorial optimization. *European Journal of Operational Research*. 2013. doi:[10.1016/j.ejor.2012.10.012](https://doi.org/10.1016/j.ejor.2012.10.012)
49. Song G, Avants BB, Gee JC. Multi-start method with prior learning for image registration. *Proceedings of the IEEE International Conference on Computer Vision*. 2007. doi:[10.1109/ICCV.2007.4409159](https://doi.org/10.1109/ICCV.2007.4409159)
50. Pérez P, De Los Campos G. Genome-wide regression and prediction with the BGLR statistical package. *Genetics*. 2014. doi:[10.1534/genetics.114.164442](https://doi.org/10.1534/genetics.114.164442)
51. Edelman A, Arias TA, Smith ST. The geometry of algorithms with orthogonality constraints. *SIAM Journal on Matrix Analysis and Applications*. 1998. doi:[10.1137/S0895479895290954](https://doi.org/10.1137/S0895479895290954)
52. Okut H, Gianola D, Rosa GJ, Weigel KA. Prediction of body mass index in mice using dense molecular markers and a regularized neural network. *Genetics Research*. 2011. doi:[10.1017/S0016672310000662](https://doi.org/10.1017/S0016672310000662)
53. Avants BB, Duda JT, Kilroy E, Krasileva K, Jann K, Kandel BT, et al. The pediatric template of brain perfusion. *Scientific data*. 2015. doi:[10.1038/sdata.2015.3](https://doi.org/10.1038/sdata.2015.3)
54. Kandel BM, Wang DJ, Gee JC, Avants BB. Eigenanatomy: Sparse dimensionality reduction for multi-modal medical image analysis. *Methods*. 2015. doi:[10.1016/j.ymeth.2014.10.016](https://doi.org/10.1016/j.ymeth.2014.10.016)
55. Tustison NJ, Cook PA, Klein A, Song G, Das SR, Duda JT, et al. Large-scale evaluation of ANTs and FreeSurfer cortical thickness measurements. *NeuroImage*. 2014. doi:[10.1016/j.neuroimage.2014.05.044](https://doi.org/10.1016/j.neuroimage.2014.05.044)
56. Franke K, Gaser C. Ten years of brainage as a neuroimaging biomarker of brain aging: What insights have we gained? 2019. doi:[10.3389/fneur.2019.00789](https://doi.org/10.3389/fneur.2019.00789)
57. O'Connell MJ, Lock EF. R.JIVE for exploration of multi-source molecular data. *Bioinformatics*. 2016. doi:[10.1093/bioinformatics/btw324](https://doi.org/10.1093/bioinformatics/btw324)
58. Tustison NJ, Avants BB, Cook PA, Kim J, Whyte J, Gee JC, et al. Logical circularity in voxel-based analysis: Normalization strategy may induce statistical bias. *Human Brain Mapping*. 2014. doi:[10.1002/hbm.22211](https://doi.org/10.1002/hbm.22211)

59. Avants BB, Duda JT, Kilroy E, Krasileva K, Jann K, Kandel BT, et al. The pediatric template of brain perfusion. *Scientific data*. 2015;2. doi:[10.1038/sdata.2015.3](https://doi.org/10.1038/sdata.2015.3)
60. Purcell S, Neale B, Todd-Brown K, Thomas L, Ferreira MAR, Bender D, et al. PLINK: A Tool Set for Whole-Genome Association and Population-Based Linkage Analyses. *The American Journal of Human Genetics*. 2007. doi:[10.1086/519795](https://doi.org/10.1086/519795)
61. Schmaal L, Hibar DP, Sämann PG, Hall GB, Baune BT, Jahanshad N, et al. Cortical abnormalities in adults and adolescents with major depression based on brain scans from 20 cohorts worldwide in the ENIGMA Major Depressive Disorder Working Group. *Molecular Psychiatry*. 2017. doi:[10.1038/mp.2016.60](https://doi.org/10.1038/mp.2016.60)
62. Tzourio-Mazoyer N, Landeau B, Papathanassiou D, Crivello F, Etard O, Delcroix N, et al. Automated anatomical labeling of activations in SPM using a macroscopic anatomical parcellation of the MNI MRI single-subject brain. *Neuroimage*. 2002;15: 273–289. doi:[10.1006/nimg.2001.0978](https://doi.org/10.1006/nimg.2001.0978)